

Effect of lithographically-induced strain relaxation on the magnetic domain configuration in microfabricated epitaxially grown $\text{Fe}_{81}\text{Ga}_{19}$

R. Beardsley¹, D. E. Parkes¹, J. Zemen², S. Bowe^{1,3}, K.W. Edmonds¹, C. Reardon⁴, F. Maccherozzi³, I. Isakov^{2,5}, P. A. Warburton⁵, R. P. Campion¹, B.L. Gallagher, S. A. Cavill^{4,3}* & A. W. Rushforth¹*

¹*School of Physics and Astronomy, University of Nottingham, Nottingham NG7 2RD, United Kingdom.*

²*Department of Physics, Blackett Laboratory, Imperial College, Prince Consort Road, London SW7 2AZ, United Kingdom*

³*Diamond Light Source Chilton, Didcot, Oxfordshire OX11 0DE United Kingdom.*

⁴*Department of Physics, University of York, Heslington, York, YO10 5DD, United Kingdom*

⁵*London Centre of Nanotechnology, University College London, London, WC1H 0AH, United Kingdom*

* Corresponding authors to whom requests for information and materials should be addressed.

We investigate the role of lithographically-induced strain relaxation in a micron-scaled device fabricated from the magnetostrictive alloy $\text{Fe}_{81}\text{Ga}_{19}$. The strain relaxation due to lithographic patterning induces a magnetic anisotropy that competes with the magnetocrystalline and shape induced anisotropy to play a crucial role in stabilising a flux-closing domain pattern. We use magnetic imaging, micromagnetic calculations and linear elastic modelling to investigate a region close to the edges of an etched structure. This highly-strained edge region has a significant influence on the magnetic domain configuration due to an induced magnetic anisotropy resulting from the inverse magnetostriction effect. Understanding this behaviour will be important when designing hybrid magneto-electric spintronic devices based on highly magnetostrictive materials.

Many existing and proposed spintronic device concepts make use of magnetic domains and domain walls to store and process data. Examples include magnetoresistive random access memory ^{1, 2}, racetrack memory ^{3, 4} and domain wall logic architectures ⁵. The drive to develop these technologies has led to a large and growing body of work on the behaviour and structure of magnetic domain configurations and domain walls ⁶.

The majority of recent studies have used electrical currents to manipulate magnetization, typically by spin transfer torque ⁷ or by magnetic field ⁸. Whilst these methods have received significant attention they have not yet adequately addressed the problem of Joule heating, which presents an increasing problem as logic and memory devices are reduced in size. It has been shown that using electric fields to manipulate magnetization can be many times more efficient than electrical current, due to the achieved reduction in power dissipation within the device^{9, 10}. Hybrid ferromagnet/piezoelectric devices, in which magnetic anisotropy is controlled by voltage induced strain, are increasingly being seen as a viable and pragmatic solution to the problem of electrical control of magnetization for spintronic applications ^{11, 12}. One of the key elements of such hybrid devices is a magnetostrictive ferromagnetic material, of which $\text{Fe}_{81}\text{Ga}_{19}$ has the highest magnetostriction coefficient for non-rare-earth containing materials ¹³, and displays highly

magnetostrictive behaviour in the form of thin films¹⁴, making it an excellent candidate for integration into the hybrid structures.

The configuration of ferromagnetic domains and domain walls in a lithographically patterned structure is determined by the balance of the anisotropy energies, including magnetocrystalline, magnetoelastic and shape-induced anisotropy terms. The relative magnitude of these different anisotropies is dependent on device size and aspect ratio. In earlier studies we have shown that the magnetization in large scale ($\sim 50 \mu\text{m}$) $\text{Fe}_{81}\text{Ga}_{19}$ structures is dominated by magnetoelastic and cubic magnetocrystalline anisotropy terms, and the domains appear disordered with domain walls forming at nucleation sites determined by imperfections in the device structure¹². In narrower devices, with width $\sim 15 \mu\text{m}$ and length $\sim 90 \mu\text{m}$, shape-induced anisotropy plays a more important role and magnetic domains form a pattern which minimises the stray field from the device¹⁵. In this letter we discuss an additional contribution to the anisotropy energy which can result from the relaxation of growth strain at the edges of lithographically patterned bars when the width is reduced to the order of $1 \mu\text{m}$. This strain-relaxation originates from a lattice mismatch between the epitaxially grown magnetic layer and the substrate. The lattice mismatch imposes a built in compressive strain in the magnetic layer, which can be relaxed by etching of the continuous film into patterned devices. The effect of strain-relaxation on magnetic anisotropy was studied extensively in the diluted magnetic semiconductor GaMnAs ^{16, 17, 18, 19}. There, the low magnetic moment prevented the formation of regular domain patterns and the observations were interpreted using a single domain model. In our high moment $\text{Fe}_{81}\text{Ga}_{19}$ devices this additional contribution to the magnetic anisotropy energy results in the stabilisation of a flux closure magnetic domain pattern, which is distorted compared to the pattern observed in wider bars¹⁵ where the effects of the lattice relaxation are less significant.

The sample consisted of a 14.3 nm $\text{Fe}_{81}\text{Ga}_{19}$ epitaxial thin film grown by molecular beam epitaxy on a 500 nm Si-doped buffer on a $\text{GaAs}(001)$ substrate. A 1.5 nm amorphous GaAs capping layer was grown to protect the metallic layer from oxidation. The layer structure is shown in Figure 1 (a). X-ray diffraction measurements using a Phillips X-Pert materials research diffractometer on material grown under similar conditions¹⁴ show a single peak corresponding to the $\text{Fe}_{81}\text{Ga}_{19}$ layer, indicating that the layer is a single crystal phase with a vertical lattice parameter of $a_{\perp}^{\text{FeGa}} = 0.296 \text{ nm}$. The lattice constant of the A2 phase of single crystal bulk $\text{Fe}_{81}\text{Ga}_{19}$ is known to be $a_o^{\text{FeGa}} = 0.287 \text{ nm}$.²⁰ Taking the in plane lattice constant of a fully strained film to be half the GaAs substrate lattice parameter ($a_{\parallel}^{\text{FeGa}} = 0.5a_o^{\text{GaAs}} = 0.283 \text{ nm}$) and assuming a Poisson ratio of 0.45 ²¹ this would imply that the out of plane lattice constant of a fully strained $\text{Fe}_{81}\text{Ga}_{19}$ film on GaAs would be 0.296 nm , consistent with the measured value. Superconducting quantum interference device (SQUID) magnetometry shows that the cubic magnetocrystalline anisotropy favouring the $[100]/[010]$ directions has a magnitude $K_C = 18.9 \times 10^3 \text{ J/m}^3$ for the unpatterned film, and the weaker uniaxial anisotropy favouring the $[110]$ direction is $K_U = 12.4 \times 10^3 \text{ J/m}^3$. The saturation magnetisation of the film is $1.4 \times 10^6 \text{ A/m}$. An L-shaped structure with arms of width $1.2 \mu\text{m}$ and length $10 \mu\text{m}$ along the $[100]/[010]$ directions was fabricated using electron beam lithography and Ar ion milling. The milled depth was greater than the film thickness which resulted in a 100 nm GaAs mesa, measured by atomic force microscopy, with the $\text{Fe}_{81}\text{Ga}_{19}$ and capping layers on top (Figure 1 (a)). In this letter we focus on the behaviour in one $10 \mu\text{m}$ -long arm of the L-shaped structure.

Finite element calculations were used to gain insight into the structural behaviour of a bar of infinite length and the same cross-sectional dimensions as the experimental device. A fixed structural

constraint was set at the substrate boundaries and an initial in-plane compressive strain of $(a_0^{FeGa} - a_{||}^{FeGa})/a_0^{FeGa} = 1.4\%$ was included in the $Fe_{81}Ga_{19}$ layer. The strain profiles in the wire cross section were calculated using a partial differential equation solver (the COMSOL software package) implementing the theory of an anisotropic elastic medium. From here on we define positive strain as the difference between the in-plane lattice spacing along the directions perpendicular and parallel to the stripe such that the zero strain state corresponds to the unrelaxed film.

Figures 1(a) and 1(b) show the calculated strain relaxation across the wire cross-section, defined as $(\epsilon_{xx} - \epsilon_{yy})$ where ϵ_{xx} and ϵ_{yy} are the in-plane components of strain in directions perpendicular and parallel to the wire. The strain profile at the $Fe_{81}Ga_{19}$ / cap interface, shown in Figure 1(c), reveals that there is a nonzero strain relaxation in the centre of the cross-section, which increases in amplitude away from the bar centre. The relaxation in the edge-region was also seen in the previous studies on (Ga,Mn)As-based devices¹⁶⁻¹⁹. An interesting feature of this profile is the abrupt decrease in amplitude in the regions near to the edges of the bar. This discontinuity is only observed with the inclusion of the GaAs capping layer, which tends to suppress the relaxation of the in-built strain by partially clamping the top surface as shown in Figure 1 (b).

Magnetic domains were imaged using photoemission electron microscopy (PEEM) on beamline I06 of the Diamond Light Source²². Illuminating the sample at oblique incidence and making use of X-ray magnetic circular dichroism at the Fe L_3 edge as the contrast mechanism allowed sensitivity to in-plane moments with a spatial resolution of approximately 50 nm. Figure 2 (a) shows an image of the domain configuration in a $1.2 \mu m \times 6 \mu m$ section of the bar. The flux-closure domain configuration observed is different to that seen in previous studies of wires with width $15 \mu m$ ¹⁵ in that the regions with magnetisation perpendicular to the length of the bar are broadened at the edges of the bar. In this study there is no externally induced strain and we attribute the observed domain behaviour to the relatively large effect of non-linear strain relaxation at the bar edges in our narrower device.

To understand the experimentally observed domain configuration we performed micromagnetic calculations carried out using the Object Oriented Micromagnetic Framework (OOMMF)²³. The simulation used magnetocrystalline anisotropy coefficients determined by the SQUID magnetometry measurements of the unpatterned $Fe_{81}Ga_{19}$ film, a cell size of $4nm \times 4nm \times 10nm$ and critical damping. The OOMMF simulation was initialised in a flux-closing state, with flux-closing units having an aspect ratio of 1:1.3, which is the average aspect ratio present in the experimental image.

The magneto-elastic coupling present in the $Fe_{81}Ga_{19}$ film leads to a strain-induced uniaxial anisotropy across the width of the bar, with a profile determined by the strain profile shown in Figure 1 (c). The relation between strain and magneto-elastic anisotropy energy is, $\Delta K_{me} = B_{me}\epsilon$, where ΔK_{me} represents the change in the magnetic anisotropy energy and ϵ is the position dependent uniaxial strain perpendicular to the bar length. We set the magneto-elastic constant, $B_{me} = 1.56 \times 10^7 \text{ J/m}^3$ as determined previously for an epitaxial thin $Fe_{81}Ga_{19}$ film¹⁴. We have approximated the anisotropy energy as a function of position by fitting a first order polynomial to the edge region, and an exponential function to the central region of the calculated strain profile. This strain-induced anisotropy energy was incorporated into the OOMMF calculation as an additional uniaxial magnetocrystalline anisotropy term, with the anisotropy axis perpendicular to the length of the bar. The results of micromagnetic calculations based on the approximated anisotropy

profile are shown in Figure 2(b). Similar to the experimental data, the ground state is a flux-closure pattern with regions magnetised perpendicular to the length of the bar. To observe broadening of the domain boundaries at the edges of the bar to an extent similar to that observed in the experimental data, we scale the magnitude of the strain-induced anisotropy by a factor of 0.4 in the simulations, otherwise the calculated broadening is too large. A possible explanation for the need to scale the anisotropy might arise from damage to the $\text{Fe}_{81}\text{Ga}_{19}$ layer at the edges of the bar during device fabrication, which would degrade the magnetism in the region where the strain relaxation is largest. Figure 2(c) shows a calculation without the additional strain-induced anisotropy. This calculation reveals that the bar will not support the regular flux closure domain configuration in the absence of the strain-induced anisotropy due to the dominant role of the shape-induced anisotropy. Calculations on bars with the same $1.2\text{ }\mu\text{m}$ width, but using periodic boundary conditions to simulate infinite length (Figure 2(d)) reveal that a very similar flux closure pattern represents the lowest energy ground state when the strain induced anisotropy is included, but that without this anisotropy term a single domain configuration with magnetisation pointing along the length of the bar is the lowest energy configuration.

In our $\text{Fe}_{81}\text{Ga}_{19}$ structures the cubic magnetocrystalline anisotropy supports magnetic easy axes along the [100] and [010] directions. The small intrinsic uniaxial anisotropy along the [110] direction acts to distort the shape of the magnetic domains and leads to a canting of the magnetic moments towards the [110] direction. This feature is present in the experimental data (Figure 2(a)) and is also revealed in the calculations (Figures 2(b) and (d)). Furthermore, the magnetostriction constant in $\text{Fe}_{81}\text{Ga}_{19}$ is largest along the [100]/[010] directions, hence magneto-elastic effects will be maximised by strain relaxation along these directions²¹, as is the case with our device.

In conclusion we have demonstrated that relaxation of growth strain is an important factor in determining the magnetic domain configuration of micron sized devices based on $\text{Fe}_{81}\text{Ga}_{19}$. In the $1.2\text{ }\mu\text{m}$ wide bars investigated, the strain-induced anisotropy stabilises the formation of a regular flux-closure domain configuration and distorts the features near the edges of the bar. Growth strain is an additional degree of freedom to be controlled or manipulated in the design of nanoscale magnetic devices. The strain relaxation is largest in the region around 50-100nm from the edges of the structure, therefore, the induced anisotropy will be of increasing importance when devices are scaled to the sub-micron regime.

The authors would like to acknowledge Diamond Light Source for the provision of beamtime under SI-8560 and 7601. AWR acknowledges funding for an EPSRC Career Acceleration Fellowship (EP/H003487/1). We are grateful for access to the University of Nottingham High Performance Computing Facility.

Author Contributions

RB, DEP, SB, KWE, FM, SAC and AWR conducted the PEEM measurements. RB, DEP and CR performed electron beam lithography. II carried out ion milling. JZ performed structural calculations of the strain profile using the COMSOL package. DEP carried out the micromagnetic simulations. RPC was responsible for the growth of the semiconductor and metallic layers. All authors contributed to writing the manuscript.

Figure Captions

Figure 1

(a) Cross-sectional view of the layer structure of the experimental device and simulated colour scale map showing the relaxation of the growth strain as a function of depth in the bar. (b) A zoomed section of the colour scale map showing the relaxation of the growth strain as a function of depth in the edge region of the bar. (c) The simulated strain profile across the $\text{Fe}_{81}\text{Ga}_{19}$ bar at the $\text{Fe}_{81}\text{Ga}_{19}$ /cap interface.

Figure 2

(a) Experimental top down PEEM image of $1.2\text{ }\mu\text{m} \times 6\text{ }\mu\text{m}$ region of a bar with arrows indicating the magnetization direction. (b) Micromagnetic simulation for the $1.2\text{ }\mu\text{m} \times 6\text{ }\mu\text{m}$ bar with an anisotropy profile that includes the calculated strain relaxation profile scaled by a factor of 0.4. (c) Micromagnetic simulation for the $1.2\text{ }\mu\text{m} \times 6\text{ }\mu\text{m}$ bar without the inclusion of a strain induced anisotropy. (d) As in (b), but including periodic boundary conditions along the [100] axis to represent a bar of infinite length.

Figure 1

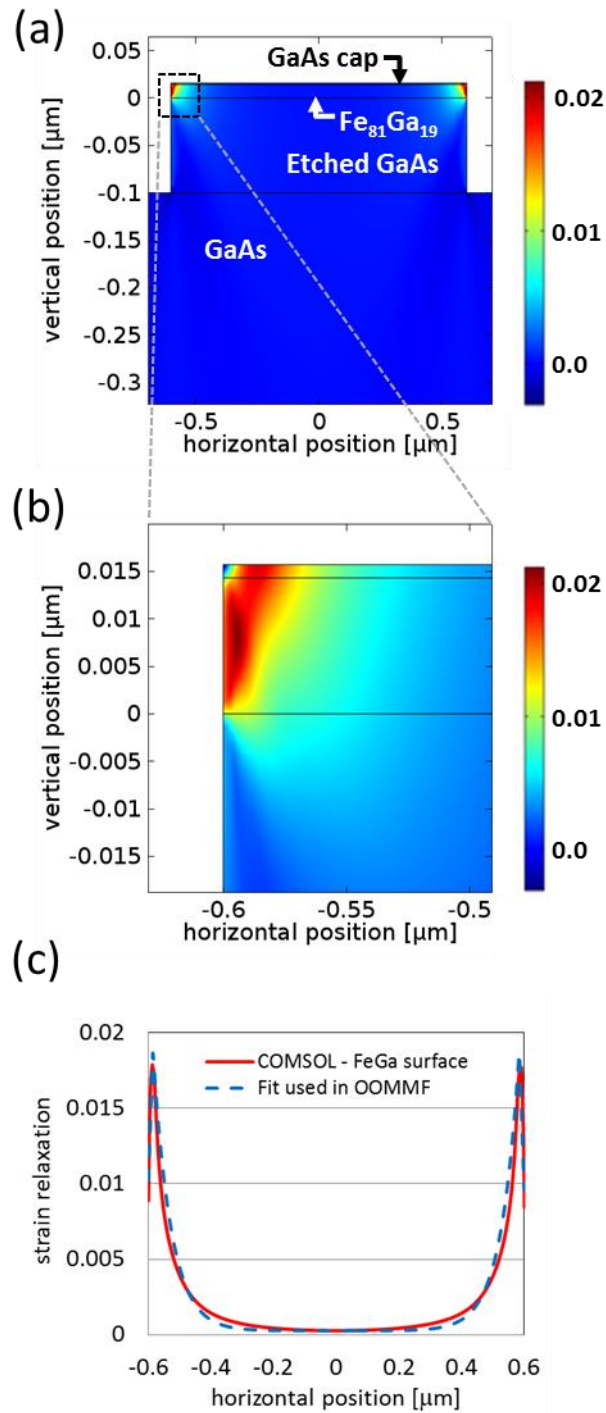
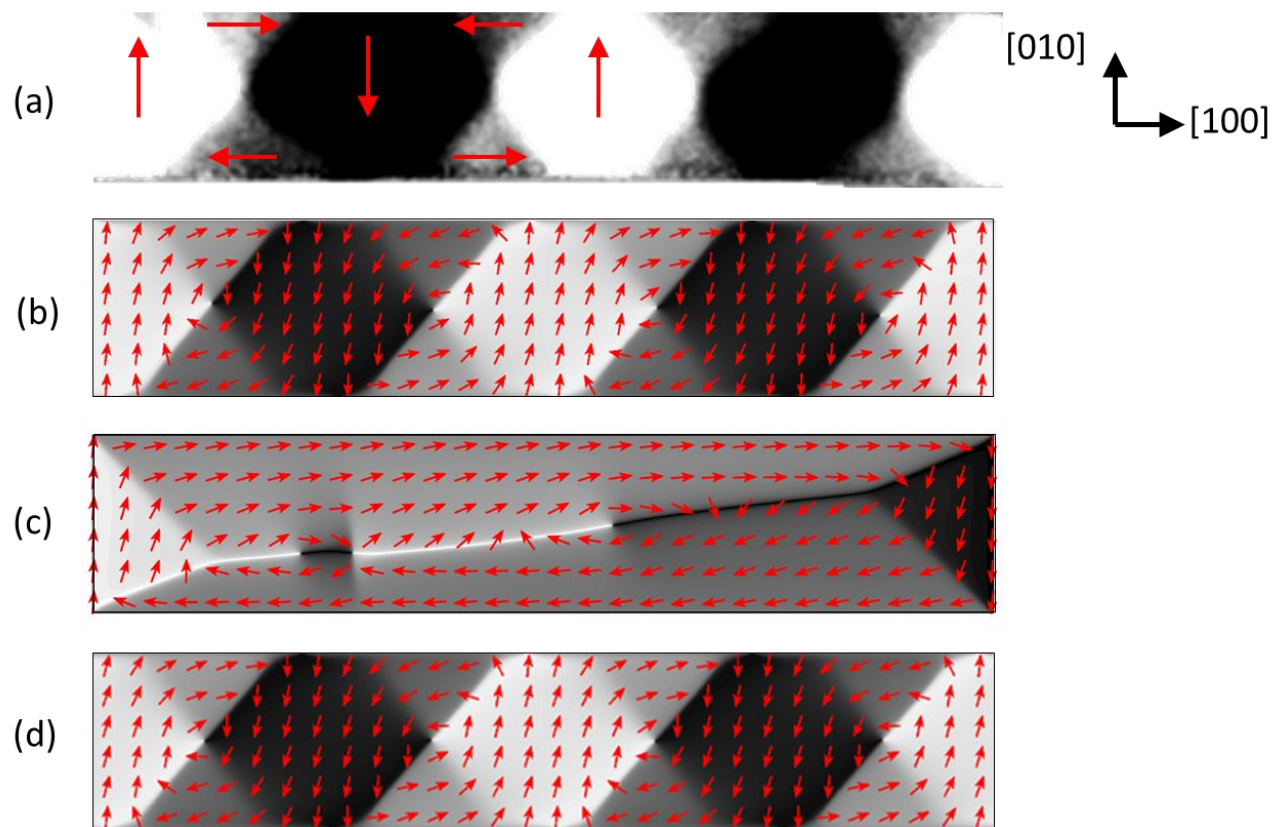


Figure 2



1. Fukami S, *et al.* Low-current perpendicular domain wall motion cell for scalable high-speed MRAM. In: *VLSI Technology, 2009 Symposium* (2009).
2. Gallagher WJ, Parkin SSP. Development of the magnetic tunnel junction MRAM at IBM: From first junctions to a 16-Mb MRAM demonstrator chip. *IBM Journal of Research and Development* **50**, 5-23 (2006).
3. Parkin S. Racetrack memory device. US Patent 6834005 (2012).
4. Parkin SSP, Hayashi M, Thomas L. Magnetic Domain-Wall Racetrack Memory. *Science* **320**, 190-194 (2008).
5. Allwood DA, Xiong G, Faulkner CC, Atkinson D, Petit D, Cowburn RP. Magnetic Domain-Wall Logic. *Science* **309**, 1688-1692 (2005).
6. Ruediger U, Yu J, Zhang S, Kent AD, Parkin SSP. Negative Domain Wall Contribution to the Resistivity of Microfabricated Fe Wires. *Physical Review Letters* **80**, 5639-5642 (1998).
7. De Ranieri E, *et al.* Piezoelectric control of the mobility of a domain wall driven by adiabatic and non-adiabatic torques. *Nat Mater* **12**, 808-814 (2013).
8. Beach GSD, Nistor C, Knutson C, Tsoi M, Erskine JL. Dynamics of field-driven domain-wall propagation in ferromagnetic nanowires. *Nat Mater* **4**, 741-744 (2005).
9. Hu J-M, Li Z, Chen L-Q, Nan C-W. High-density magnetoresistive random access memory operating at ultralow voltage at room temperature. *Nat Commun* **2**, 553 (2011).
10. Roy K, Bandyopadhyay S, Atulasimha J. Hybrid spintronics and straintronics: A magnetic technology for ultra low energy computing and signal processing. *Applied Physics Letters* **99**, - (2011).
11. Lei N, *et al.* Strain-controlled magnetic domain wall propagation in hybrid piezoelectric/ferromagnetic structures. *Nat Commun* **4**, 1378 (2013).
12. Parkes DE, *et al.* Non-volatile voltage control of magnetization and magnetic domain walls in magnetostrictive epitaxial thin films. *Applied Physics Letters* **101**, (2012).
13. Clark AE, Wun-Fogle M, Restorff JB, Lograsso TA. Magnetostrictive properties of Galfenol alloys under compressive stress. *Materials transactions* **43**, 881-886 (2002).
14. Parkes DE, *et al.* Magnetostrictive thin films for microwave spintronics. *Sci Rep* **3**, 2220, (2013).
15. Cavill SA, *et al.* Electrical control of magnetic reversal processes in magnetostrictive structures. *Applied Physics Letters* **102**, 032405 (2013).
16. Wunderlich J, *et al.* Local control of magnetocrystalline anisotropy in (Ga,Mn)As microdevices: Demonstration in current-induced switching. *Physical Review B* **76**, 054424 (2007).
17. Wenisch J, *et al.* Control of Magnetic Anisotropy in (Ga,Mn)As by Lithography-Induced Strain Relaxation. *Physical Review Letters* **99**, 077201 (2007).

18. King CS, *et al.* Strain control of magnetic anisotropy in (Ga,Mn)As microbars. *Physical Review B* **83**, 115312 (2011).
19. Hoffmann F, Woltersdorf G, Wegscheider W, Einwanger A, Weiss D, Back CH. Mapping the magnetic anisotropy in (Ga,Mn)As nanostructures. *Physical Review B* **80**, 054417 (2009).
20. Bhattacharyya S, Jinschek JR, Khachaturyan A, Cao H, Li JF, Viehland D. Nanodispersed DO3-phase nanostructures observed in magnetostrictive Fe-19% Ga Galfenol alloys. *Physical Review B* **77**, 104107 (2008).
21. Clark AE, *et al.* Extraordinary magnetoelasticity and lattice softening in bcc Fe-Ga alloys. *Journal of Applied Physics* **93**, 8621-8623 (2003).
22. Dhesi SS, *et al.* The Nanoscience Beamline (I06) at Diamond Light Source. *AIP Conference Proceedings* **1234**, 311-314 (2010).
23. Donahue MJ, Porter DG. *OOMMF User's Guide, Version 1, Interagency Report NISTIR 6376*, (1999).